Journal of Power Sources 197 (2012) 253–259

Contents lists available at SciVerse ScienceDirect

Journal of Power Sources

journal homepage: www.elsevier.com/locate/jpowsour

Synthesis of the $LiFePO_4$/C core–shell nanocomposite using a nano-$FePO_4$/polythiophene as an iron source

Jing Liu[a,b,c], Guiling Yang[a,b], Xianfa Zhang[d], Jiawei Wang[a,b], Rongshun Wang[a,b,*]

[a] Institute of Functional Materials, Department of Chemistry, Northeast Normal University, Changchun, Jilin 130024, PR China
[b] LIB Engineering Laboratory, Materials Science and Technology Center, Changchun, Jilin 130024, PR China
[c] School of Chemistry and Chemical Engineering, Shandong University, Ministry of Education, Jinan 250100, PR China
[d] Key Laboratory of Functional Inorganic Material Chemistry, Ministry of Education, Heilongjiang University, Harbin 150080, PR China

ARTICLE INFO

Article history:
Received 6 June 2011
Received in revised form 9 September 2011
Accepted 12 September 2011
Available online 16 September 2011

Keywords:
Nanocomposite
Core–shell structure
High conductivity
Lithium-ion battery
Electrochemistry

ABSTRACT

For the first time, a $LiFePO_4$/C core–shell nanocomposite has been synthesized using a nano-$FePO_4$/polythiophene (PTh) as an iron source. With this method, the PTh is *in situ* polymerized to restrain the growth of $FePO_4$ particles, and the typical size of $FePO_4$/PTh particles is in the range of 20–50 nm. The optimized $LiFePO_4$/C nanocomposite is synthesized at 750 °C using 40% citric acid. The prepared $LiFePO_4$ particles show a typical size of 50–100 nm and they are fully coated by carbon of 2–4 nm thickness. The $LiFePO_4$/C core–shell nanocomposite gives an improved high electronic conductivity and a good electrochemical behavior at high rates. Thus, this novel method is an effective and facile strategy to improve the rate performance of the $LiFePO_4$ cathode.

1. Introduction

$LiFePO_4$ is one of the most promising cathode materials for next-generation lithium-ion batteries because of its many advantages, such as the high energy density, low cost, environmental friendliness and excellent thermal safety [1–4]. However, its slow lithium ion diffusion rate combined with the intrinsic poor electronic conductivity leads to a poor rate performance [1]. In recent years, considerable effort has been devoted to improve the performance of $LiFePO_4$, in terms of rate capability and lifetime, to a practical level [5–11].

Downsizing the particle size to nanoscale is an efficient strategy to enhance the lithium transport kinetics because of the drastically shortened diffusion length [12,13]. Thus, much emphasis has been placed on nano-sized $LiFePO_4$ [14,15]. Nanoparticulate $LiFePO_4$ can be obtained by many approaches, including some low-temperature techniques such as sol–gel method, co-precipitation procedure and hydrothermal process [16–21]. However, many obstacles have been encountered in the conversion from laboratory synthesis to large-scale production because of the complicated synthesis techniques and/or the hard controlled synthesis situation for these methods. Solid-state reaction is still the better choice for industrial production [22]. But for the traditional solid-state method, a main problem is that the $LiFePO_4$ particles tend to grow up under the high-temperature heat treatment. By far, few studies have been focused on the synthesis of nano-sized $LiFePO_4$ below 100 nm from a high-temperature solid-state method [23,24], and no rule has been put forward formally to ensure the repeatability.

On the other hand, although it is well known that a conductive coating can effectively enhance the electronic conductivity of $LiFePO_4$, it is rather difficult to coat $LiFePO_4$ homogeneously with a carbon shell during the formation procedure of $LiFePO_4$ at high temperature. Carbon does not cover the entire $LiFePO_4$ surface, leading to a partly coating and hence insufficient electronically conducting network [9]. To obtain better conductive network, excessive carbonaceous materials are required, which will greatly decrease the tap density of active substances in the cathodes [25,26]. Core–shell $LiFePO_4$/C is expected to combine the function of both core and shell parts and then improve the performance of the composite. However, the way to obtain the $LiFePO_4$/C core–shell nanocomposite, which has been seeking for years, is really hard to achieve, especially for a simple high-temperature solid-state method. To the best of our knowledgement, very few papers have really prepared this kind of $LiFePO_4$/C [24,27].

In this work, a successful example that combines those two strategies has been synthesized. For the first time, a

* Corresponding author at: Institute of Functional Materials, Department of Chemistry, Northeast Normal University, Changchun, Jilin 130024, PR China. Tel.: +86 431 85099511; fax: +86 431 85099511.
E-mail address: wangrs@nenu.edu.cn (R. Wang).

0378-7753/$ – see front matter © 2011 Elsevier B.V. All rights reserved.
doi:10.1016/j.jpowsour.2011.09.028

nano-$FePO_4$/PTh is used as an iron source to prepare a core–shell $LiFePO_4$/C nanocomposite. Herein, PTh is *in situ* polymerized on the surface of the generated $FePO_4$ particles to restrain their growth, as shown in Eq. (1), so the typical size of the obtained $FePO_4$ particle is restricted within 20–50 nm. Although a very small amount of Fe^{3+} was reduced to Fe^{2+} for oxidative polymerization of thiophene, the fresh Fe^{2+} would rapidly be oxidated to Fe^{3+} by a large amount of NO_3^- in the strong acid solution. Furthermore, the PTh layer will be carbonized at high temperature, which contributes greatly to the formation of carbon shell. Using the nano-$FePO_4$/PTh composite as an iron source, we optimized the synthesis process and successfully prepare a $LiFePO_4$/C core–shell nanocomposite at 750 °C. It means that a $LiFePO_4$/C core–shell nanocomposite can be prepared by controlling the morphology of precursor, i.e. $FePO_4$, using the high-temperature solid-state method. The morphology and the electrochemical performance of the prepared $LiFePO_4$/C were characterized.

$$Fe^{3+} + {PO_4}^{3-} + n(\text{thiophene}) \xrightarrow[pH=2.0]{10M HNO_3} FePO_4/\text{polythiophene} \downarrow \quad (1)$$

2. Experimental methods

2.1. Synthesis

The $FePO_4$/PTh composite was synthesized from $Fe(NO_3)_3{\cdot}9H_2O$, $(NH_4)_2HPO_4$ and thiophene monomer. In a typical synthesis, a 0.25 M $Fe(NO_3)_3$ solution was added drop by drop into the 0.25 M $(NH_4)_2HPO_4$ solution mixed with 2 ml thiophene monomer under vigorous stirring. During the whole synthesis process, a 10 M HNO_3 solution was used to control the pH value around 2.0. In the strong nitric acid solution, the *in situ* oxidative polymerization reaction of thiophene took place. The $FePO_4$/PTh precipitate was washed with distilled water for several times and dried in an oven at 80 °C for 3 days.

A $LiFePO_4$/C composite was synthesized from $FePO_4$/PTh, $LiOH{\cdot}H_2O$ and citric acid. Stoichiometric of $FePO_4$/PTh and $LiOH{\cdot}H_2O$ with a suitable amount of citric acid (25–50 wt.% vs. $LiFePO_4$) were ball-milled for 10 h in the ethanol, and then dried in blast oven at 60 °C for 12 h. The thermal treatment under flowing nitrogen was performed at 450 °C for 3 h and 650–750 °C for 10 h. The final black powder was $LiFePO_4$/C composite.

2.2. Characterization

The carbon contents in $LiFePO_4$/C composites were determined by the VarioEL III (elementar, Germany) element analyzer. The electronic conductivity was measured with a Four-Point Probe Meter (SDY-5, Guangzhou) by pressing the sample in the form of disk at 20 MPa, with a diameter of 15 mm and a thickness of 1.1 mm. FT-IR analysis was performed on KBr-supported samples using a Magna 560 spectrometer (American Nicolet). The phase purity and structure were detected with powder X-ray diffraction (XRD, Bruker, D8 Advance) using Cu Kα radiation (λ = 1.5406 Å). The particle morphology was observed by scanning electron microscopy (SEM, XL 30 ESEM-FEG, FEI Company), transmission electron microscopy (TEM) and high resolution transmission electron microscopy (HRTEM, JEM-2010).

2.3. Electrochemical measurements

The electrochemical performance of the cathode was characterized in experimental cells with lithium metal as the counter electrode. The slurry with 84 wt.% host material, 8 wt.% Super P and 8 wt.% polyvinylidene fluoride (PVDF) dispersed in N-methylpyrrolidinone (NMP) was coated on Al foil and dried in a vacuum oven at 120 °C for 12 h. The resulting cathode film was pressed and punched into a disc. The $LiFePO_4$/C loading was 2–5 mg cm^{-2} in the experimental cells. Celgard 2400 was used as separator. The electrolyte was 1 M $LiPF_6$ in a mixture of ethylene carbonate (EC) and dimethyl carbonate (DMC) (1:1 volume). All cells were assembled in an argon-filled glove box and tested at room temperature over the voltage range 2.5–4.2 V. 1 C = 170 mA g^{-1}.

3. Results and discussion

3.1. Component and morphology analysis of the $FePO_4$/PTh composite

The XRD pattern of the dried precipitate (plot a) is provided in Fig. 1A. No obvious diffraction peaks can be observed, indicating an amorphous form of the prepared composite. To confirm the component, the sample was heated at 700 °C for 10 h in the air, and its XRD pattern is shown in plot b. As described in the previous literatures [28,29], the amorphous structure transforms to a crystalline form after being heated at 700 °C, indexing to be a pure trigonal, α-quartz-type $FePO_4$ (JCPDS file no. 77-0094). So the existence of amorphous $FePO_4$ in our sample can be confirmed. No diffraction peak of PTh is detected in plot b because it has been oxidized to carbon dioxide at high temperature of 700 °C in the air.

From the FT-IR spectrum of the sample in Fig. 1B, characteristic peaks of both $FePO_4$ and polythiophene can be observed. The absorption at 1050 cm^{-1} can be assigned to the asymmetric stretching vibration of P–O bonds in ${PO_4}^{3-}$ groups [30]. The peaks at around 1640 cm^{-1}, 3240 cm^{-1} and 3400 cm^{-1} are in reference to

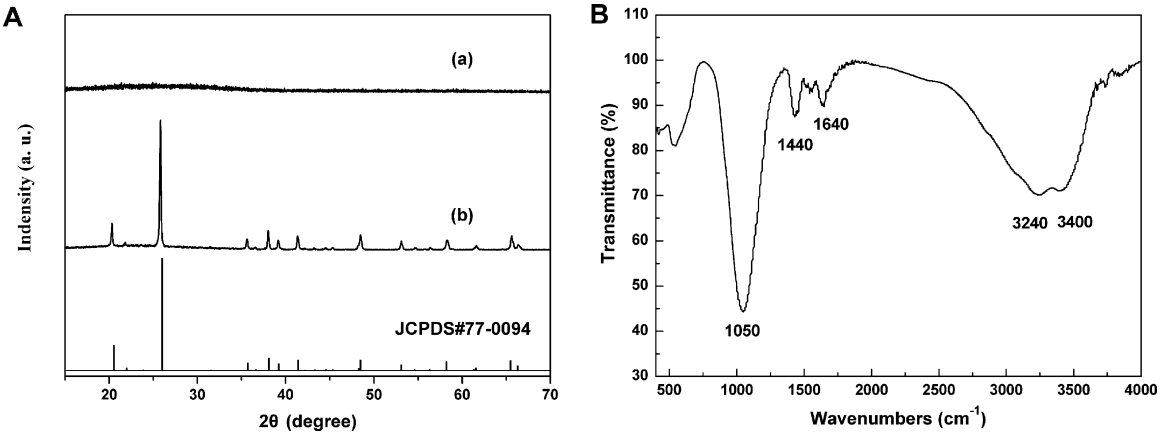

Fig. 1. XRD patterns (A) of the samples dried at 80 °C (a) and sintered at 700 °C (b); and FT-IR spectrum of the $FePO_4$/PTh composite (B).

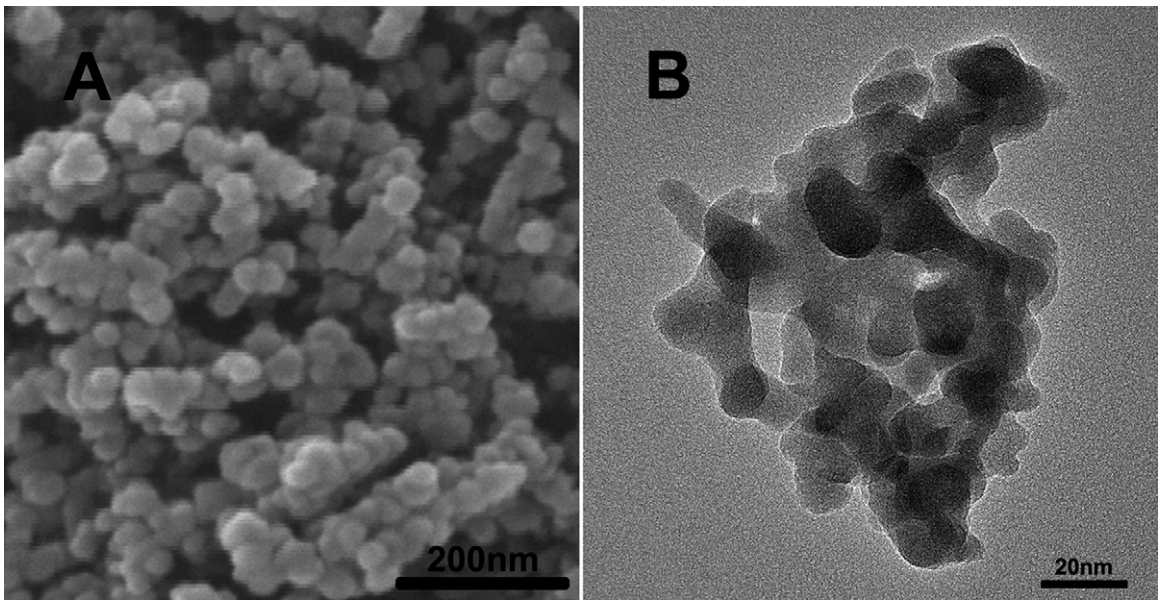

Fig. 2. SEM (A) and TEM (B) images of as-prepared $FePO_4$/PTh composite.

the bending and stretching vibrations of water molecules [31–33]. The characteristic peak at 1450 cm^{-1} corresponds to the stretching vibration modes of the thiophene ring [34]. The characteristic peak at around 1112 cm^{-1} assigned to C_α–C_α stretching vibration modes of polythiophene should be observed, although it appears to be hidden by the peak of PO_4^{3-}.

The morphology of as-prepared $FePO_4$/PTh composite is shown in Fig. 2. The SEM image in Fig. 2A shows that the $FePO_4$/PTh particles have a regular spherical shape with typical size of 20–50 nm. The TEM image shows that the material has an agglomerate structure, seen in Fig. 2B. Therefore, we have successfully synthesized a nano-$FePO_4$/PTh composite in preparation for a further synthesis of nano-$LiFePO_4$/C composite.

3.2. The effect of heating temperature on the structure and morphology of the $LiFePO_4$/C composite

To investigate the effect of heating temperature on structure and morphology of $LiFePO_4$/C composite, all the samples in this section are synthesized from 40% citric acid. Fig. 3 shows the XRD patterns of the samples synthesized at 650 °C, 700 °C and 750 °C (*Abbr.* S650, S700 and S750, respectively). In comparison with the JCPDS file (no. 83-2092), two peaks of impurity at $2\theta = 43.8°$ and 51° appear in the XRD patterns of both S650 and S700, and they are assigned to the diffraction peaks of the $Li_3Fe_2(PO_4)_3$ [35,36]. No impurity phase is detected in S750, suggesting that $Li_3Fe_2(PO_4)_3$ is reduced to $LiFePO_4$ completely under the co-work of these two kinds of carbon sources at 750 °C. Furthermore, the diffraction peaks of S750 are much stronger than those of S650 and S700, indicating a better crystallization of $LiFePO_4$.

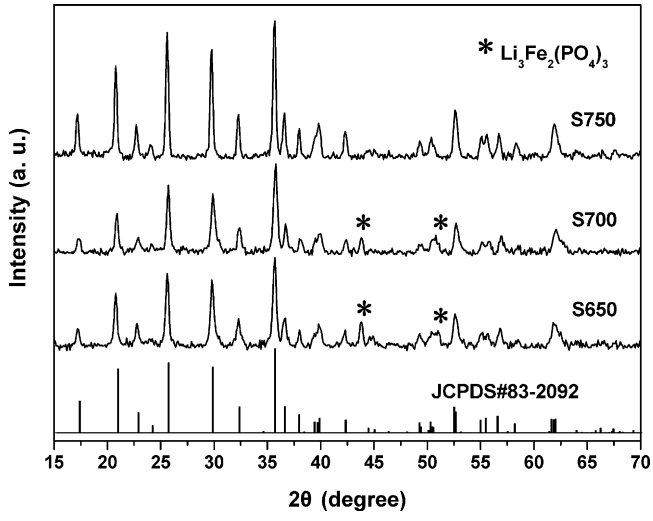

Fig. 3. XRD patterns of the $LiFePO_4$/C samples sintered at different temperatures.

The effect of heating temperature on the morphology of $LiFePO_4$ particles was also investigated by SEM. The SEM images of S650, S700 and S750 are shown in Fig. 4. As the temperature increases, although the size of $LiFePO_4$ particles appreciably grows up as reported in the literatures [37,38], S750 has a much looser structure than the other two samples.

Temperature higher than 750 °C is not discussed in this paper, because it is more energy consuming, and the capacities will decrease due to the agglomeration of the small particles into larger ones and the appeared impurities [37,39,40]. So 750 °C is chosen as the heating temperature.

3.3. The effect of the amount of citric acid on the structure and morphology of the $LiFePO_4$/C composite at 750 °C

Besides the heating temperature, we also studied the effect of the amount of citric acid on the structure and morphology of $LiFePO_4$. The samples synthesized from 25%, 30%, 40% and 50% citric acid (*Abbr.* S25, S30, S40 and S50) are obtained, and their XRD patterns are shown in Fig. 5. Two small peaks of $Li_3Fe_2(PO_4)_3$ impurity at $2\theta = 47.3°$ and 47.6° can be observed in the XRD patterns of S25 and S30. As the amount of citric acid increases to 40%, the impurity peaks cannot be observed. All the diffraction peaks in S40 and S50 are well consistent with the olivine $LiFePO_4$ in the JCPDS file (no. 83-2092), indexing to be an orthorhombic crystal structure (space group *Pnma*). However, when 50% citric acid is added, all the peaks become weaker, indicating a decrease in crystallinity of $LiFePO_4$. This should be related with the smaller particle size and more amorphous carbon content in S50 [39].

The SEM images of these four samples are shown in Fig. 6. The mean size of $LiFePO_4$ particles is observed to be decreased as the

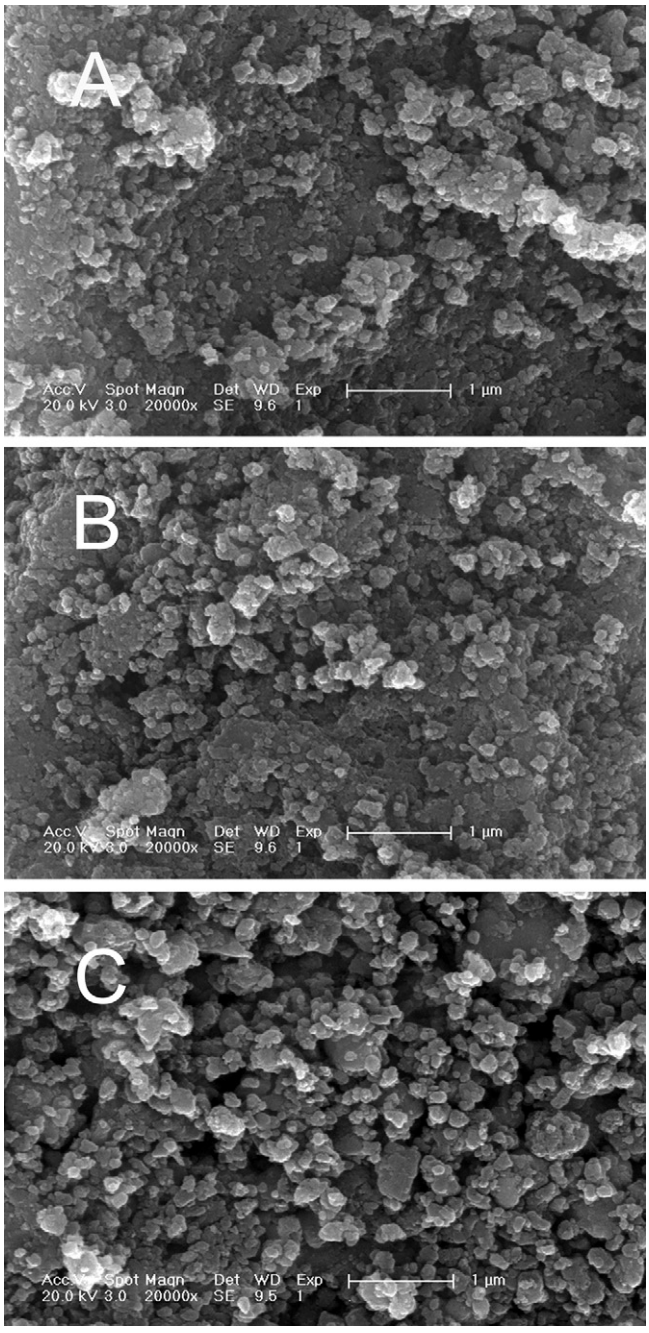

Fig. 4. SEM images of the $LiFePO_4$/C samples sintered at 650 °C (A), 700 °C (B) and 750 °C (C).

amount of citric acid increases. It is notable that S40 exhibits a most homogeneous distribution with the typical size around 100 nm, as shown in Fig. 6C. Nevertheless, the $LiFePO_4$ particles tend to badly agglomerate under a continuative addition of citric acid, as observed in Fig. 6D.

3.4. The effect of the amount of citric acid on the electrochemical performance of $LiFePO_4$/C synthesized at 750 °C

The charge–discharge curves of the S25, S30, S40 and S50 at the rate of 0.1 C are shown in Fig. 7. The discharge capacities of these samples are 91 mAh g^{-1}, 140 mAh g^{-1}, 151 mAh g^{-1} and 125 mAh g^{-1}, respectively. According to the XRD analysis, the poor electrochemical performance of S25 can be ascribed to the

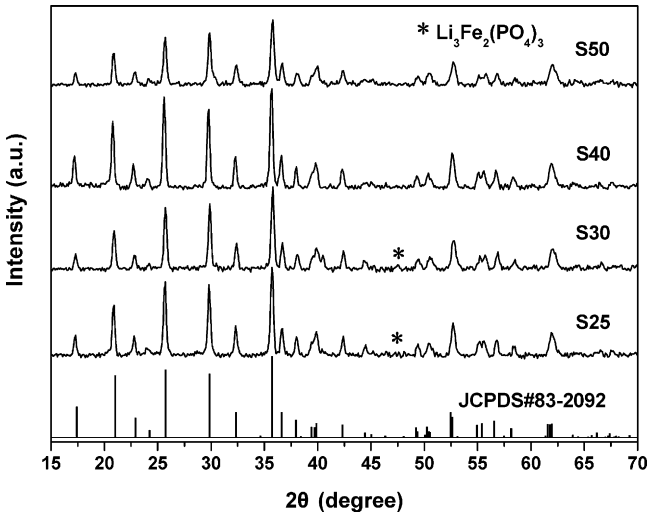

Fig. 5. XRD patterns of the $LiFePO_4$/C samples synthesized with various amount of citric acid.

relatively larger amount of $Li_3Fe_2(PO_4)_3$ impurity. It seems that the electrochemical performance becomes better with fewer impurities. However, the S50, which is observed as a single-phase $LiFePO_4$ from the XRD pattern, delivers a low discharge capacity of only 125 mAh g^{-1}. Based on the XRD and SEM analyses, we believe it should be attributed to the decreased crystallinity of $LiFePO_4$ and the serious agglomerate of particles. Meanwhile, the ΔVs, which are calculated from the differences of charge and corresponding discharge voltage plateaus, are observed as 0.1196 V, 0.0796 V, 0.0357 V and 0.0328 V for S25, S30, S40 and S50, individually, demonstrating a decreasing trend of polarization. It should be attributed to the increasing electronic conductivities of these samples, as listed in Table 1.

Table 1 gives the residual carbon contents, electronic conductivities, and discharge capacities of $LiFePO_4$/C composites synthesized from various amount of citric acid. The electronic conductivities of these samples are enhanced by the increase of residual carbon, which is in correspondence with the decrescent polarization. However, the residual conductive carbon is intrinsically an inert material for lithium-ion storage, and the increasing amount of carbon in the active material would certainly lead to capacity loss. For instance, the carbon content is 4.3% in S750, so its capacity referred to $LiFePO_4$ only is 151/(1–0.043) = 158 mAh g^{-1}. As the carbon (the content as listed in Table 1) is neglected, the discharge capacities of these samples at the rate of 0.1 C are 93 mAh g^{-1}, 144 mAh g^{-1}, 158 mAh g^{-1} and 132 mAh g^{-1}, respectively. Therefore, the $LiFePO_4$/C composite synthesized at 750 °C using 40% citric acid is the best choice.

3.5. Morphology and electrochemical study of the optimized $LiFePO_4$/C composite

The TEM and HRTEM images of the $LiFePO_4$/C composite prepared under the optimal synthesis condition are shown in Fig. 8. Fig. 8A shows a TEM image including several primary particles and it illustrates that the typical size of $LiFePO_4$ particles is in the range of 50–100 nm. The selected-area electron diffraction (SAED) pattern inserted in Fig. 8A suggests that the prepared $LiFePO_4$ is highly crystalline. The carbon distributed in the interspaces of $LiFePO_4$ particles can also be observed clearly. The carbon on the surface of $LiFePO_4$ particles (the region in the red rectangle) is observed by HRTEM, as shown in Fig. 8B. It can be observed that they are completely coated on the surface of highly crystalline $LiFePO_4$ particles with about 2–4 nm thickness. The single particle in Fig. 8C shows

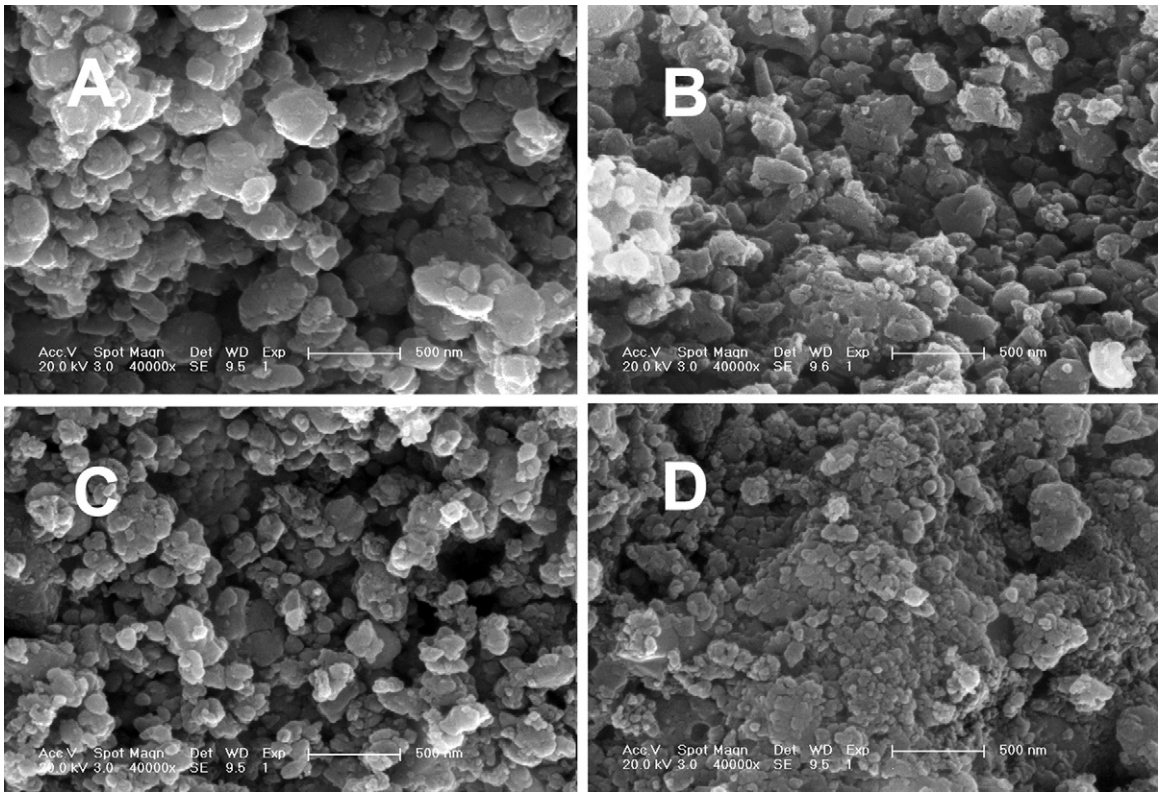

Fig. 6. SEM images of the $LiFePO_4$/C samples synthesized with 25% (A), 30% (B), 40% (C) and 50% (D) citric acid.

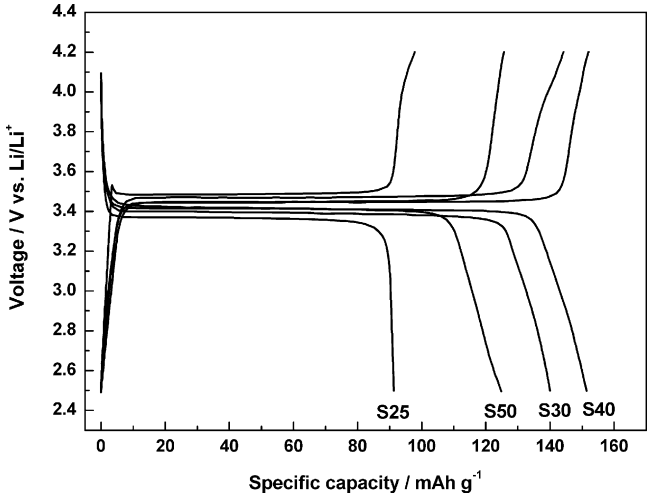

Fig. 7. The charge–discharge curves of the $LiFePO_4$/C samples synthesized with various amount of citric acid at the rate of 0.1 C.

that the carbon is fully coated on the surface of $LiFePO_4$ crystallite, forming a $LiFePO_4$/C core–shell structure. The carbon in the boundary/interspace of $LiFePO_4$ particles ensures that each spot on the particle surface is able to accept the electron rapidly, which can also contribute to an increase in the electrical continuity between $LiFePO_4$ crystallites.

Galvanostatic charge and discharge measurements of the optimized $LiFePO_4$/C composite were carried out, as shown in Fig. 9A. Herein the charge–discharge capacities at all rates are calculated by neglecting the residual carbon. At a high rate of 10 C, the prepared $LiFePO_4$/C composite shows a discharge capacity of 103 mAh g^{-1}, demonstrating a promising rate performance. Its cycling performance at various rates is given in Fig. 9B. At rates of 0.1 C, 1 C, 2 C, 5 C and 10 C, all the discharge capacities keep almost constants with little fading up to 100 cycles. At a high rate of 5 C, it provides a long-term cyclability with capacity retention of over 92% after 1000 cycles, and the coulombic efficiency calculated from the discharge capacity/charge capacity remains close to 100%. These excellent electrochemical performances of $LiFePO_4$/C cathode should be attributed to the small particle size, good crystallization and the uniform carbon coating.

Table 1
Residual carbon contents, electronic conductivities, and discharge capacities of $LiFePO_4$/C composites synthesized with various amount of citric acid.

Samples	Residual carbon content (%)	Electronic conductivity (S cm^{-1})	Discharge capacity (mAh g^{-1}, $LiFePO_4$/C)	Discharge capacity (mAh g^{-1}, $LiFePO_4$)
S25	2.4	0.065	91	93
S30	3.1	0.25	140	144
S40	4.3	0.32	151	158
S50	5.2	0.57	125	132

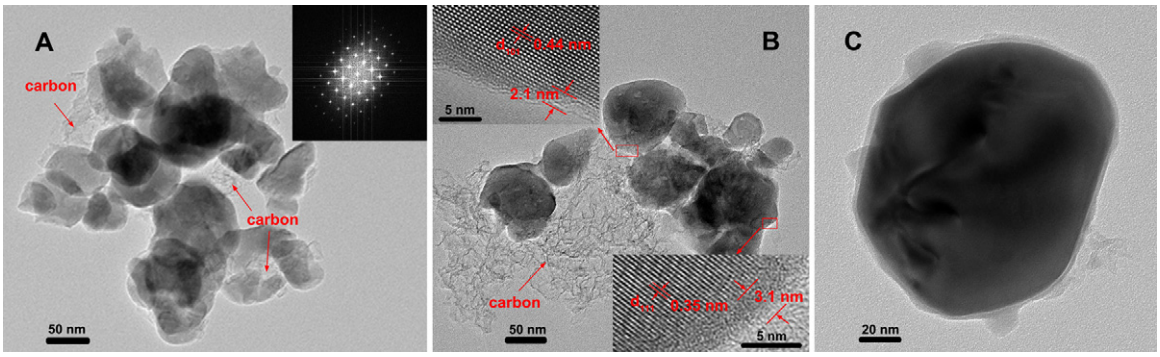

Fig. 8. TEM and HRTEM images of the optimized $LiFePO_4$/C composite.

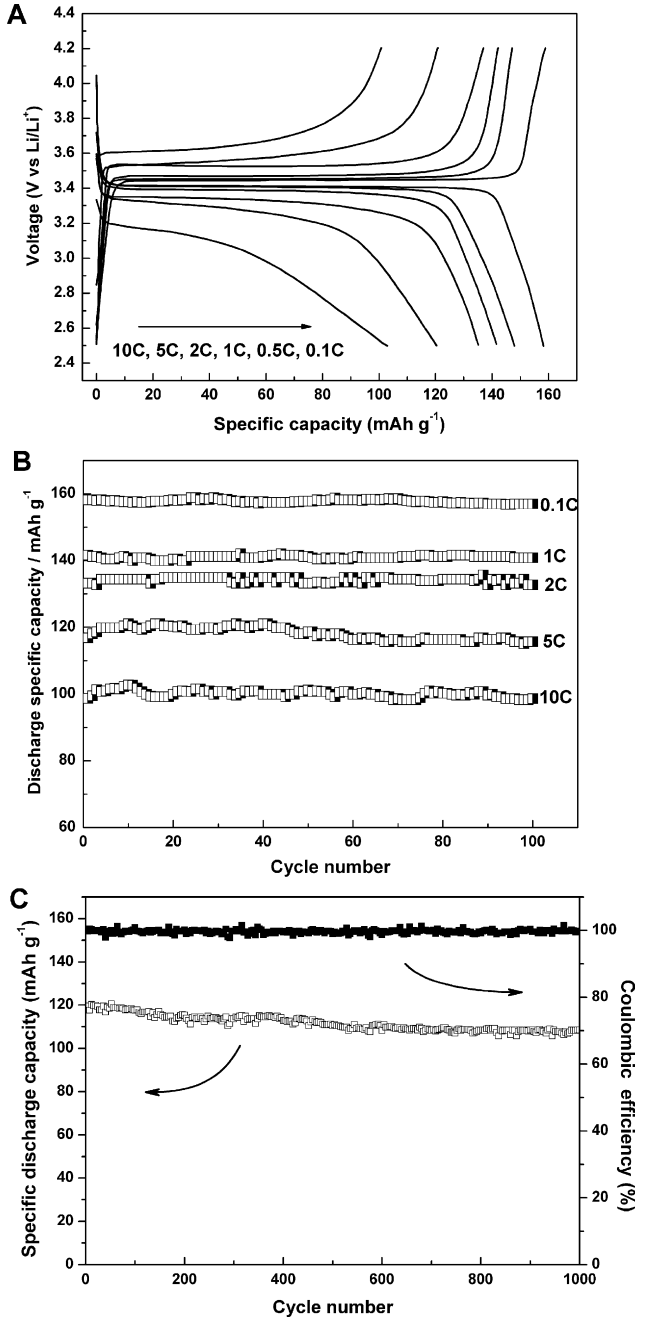

Fig. 9. Electrochemical performance of the optimized $LiFePO_4$/C composite: charge–discharge curves at different rates (A), cycle performance at different rates (B), and the long-term cyclability at the rate of 5 C.

4. Conclusions

In this work, a nano-$FePO_4$/PTh has been used as an iron source to synthesize a nano-sized $LiFePO_4$/C composite. Experimental results show that the $LiFePO_4$/C composite prepared at 750 °C using 40% citric acid shows the best physical property and electrochemical performance. The highly crystalline of $LiFePO_4$, the small particle size and the fully coated conductive carbon, give rise to an effective enhancement of its electrochemical performance. We believe our demonstration of this novel method provides an efficient strategy for other electrode materials towards nanoengineering and high conductivity.

Acknowledgement

This work was supported by a project issued by the National Key Technologies R&D Program (Grant No. 2009BAG19B00).

References

[1] A.K. Padhi, K.S. Nanjundaswamy, J.B. Goodenough, J. Electrochem. Soc. 144 (1997) 1188–1194.
[2] B.L. Ellis, K.T. Lee, L.F. Nazar, Chem. Mater. 22 (2010) 691–714.
[3] Y. Zhou, J. Wang, Y. Hu, R. O'Hayre, Z. Shao, Chem. Commun. 46 (2010) 7151–7153.
[4] S. Ferrari, R.L. Lavall, D. Capsoni, E. Quartarone, A. Magistris, P. Mustarelli, P. Canton, J. Phys. Chem. C 114 (2010) 12598–12603.
[5] S.-Y. Chung, J.T. Bloking, Y.M. Chiang, Nat. Mater. 1 (2002) 123–128.
[6] Y. Lu, J. Shi, Z. Guo, Q. Tong, W. Huang, B. Li, J. Power Sources 194 (2009) 786–793.
[7] M.-H. Lee, J.-Y. Kim, H.-K. Song, Chem. Commun. 46 (2010) 6795–6797.
[8] Z. Lu, H. Cheng, M. Lo, C.Y. Chung, Adv. Funct. Mater. 17 (2007) 3885–3896.
[9] Y.-S. Hu, Y.-G. Guo, R. Dominko, M. Gaberscek, J. Jamnik, J. Maier, Adv. Mater. 19 (2007) 1963–1966.
[10] N. Ravert, Y. Chouinard, J.F. Magnan, S. Besner, M. Gauthier, M. Armand, J. Power Sources 97–98 (2001) 503–507.
[11] W.-J. Zhang, J. Power Sources 196 (2011) 2962–2970.
[12] S. Yang, X. Zhou, J. Zhang, Z. Liu, J. Mater. Chem. 20 (2010) 8086–8091.
[13] M. Konarova, I. Taniguchi, J. Power Sources 195 (2010) 3661–3667.
[14] F. Cheng, J. Liang, Z. Tao, J. Chen, Adv. Mater. 23 (2011) 1695–1715.
[15] P.G. Bruce, B. Scrosati, J.-M. Tarascon, Angew. Chem. Int. Ed. 47 (2008) 2930–2946.
[16] Y. Liu, C. Cao, J. Li, Electrochim. Acta 55 (2010) 3921–3926.
[17] Y. Ding, Y. Jiang, F. Xu, J. Yin, H. Ren, Q. Zhuo, Z. Long, P. Zhang, Electrochem. Commun. 12 (2010) 10–13.
[18] B. Ellis, W.H. Kan, W.R.M. Makahnouk, L.F. Nazar, J. Mater. Chem. 17 (2007) 3248–3254.
[19] G. Meligrana, C. Gerbaldi, A. Tuel, S. Bodoardo, N. Penazzi, J. Power Sources 160 (2006) 516–522.
[20] D.-H. Kim, J. Kim, Electrochem. Solid-State Lett. 9 (2006) A439–A442.
[21] Y. Zhang, H. Feng, X. Wu, L. Wang, A. Zhang, T. Xia, H. Dong, M. Liu, Electrochim. Acta 54 (2009) 3206–3210.
[22] B. Kang, G. Ceder, Nature 458 (2009) 190–193.
[23] J. Liu, F. Liu, G. Yang, X. Zhang, J. Wang, R. Wang, Electrochim. Acta 55 (2010) 1067–1071.
[24] Y. Wang, Y. Wang, E. Hosono, K. Wang, H. Zhou, Angew. Chem. Int. Ed. 47 (2008) 7461–7465.
[25] Z. Chen, J.R. Dahn, J. Electrochem. Soc. 149 (2002) A1184–A1189.
[26] X.-L. Wu, L.-Y. Jiang, F.-F. Cao, Y.-G. Guo, L.-J. Wan, Adv. Mater. 21 (2009) 2710–2714.

[27] F. Pan, W. Wang, H. Li, X. Xin, Q. Chang, W. Yan, D. Chen, Electrochim. Acta 56 (2011) 6940–6944.
[28] Y. Song, P.Y. Zavalij, M. Suzuki, M.S. Whittingham, Inorg. Chem. 41 (2002) 5778–5786.
[29] Y. Song, S. Yang, P.Y. Zavalij, M.S. Whittingham, Mater. Res. Bull. 37 (2002) 1249–1257.
[30] A.A. Salah, P. Jozwiak, J. Garbarczyk, K. Benkhouja, K. Zaghib, F. Gendron, C.M. Julien, J. Power Sources 140 (2005) 370–375.
[31] K. Zaghiba, C.M. Julien, J. Power Sources 142 (2005) 279–284.
[32] S. Okada, T. Yamamoto, Y. Okazaki, J.-I. Yamaki, M. Tokunaga, T. Nishida, J. Power Sources 146 (2005) 570–574.
[33] S. Scaccia, M. Carewska, A.D. Bartolomeo, P.P. Prosini, Thermochim. Acta 383 (2002) 145–152.
[34] S. Geetha, D.C. Trivedi, Synth. Met. 155 (2005) 232–239.
[35] M. Sato, S. Tajimi, H. Okawa, K. Uematsu, K. Toda, Solid State Ionics 152–153 (2002) 247–251.
[36] K. Nagamine, K. Hirose, T. Honma, T. Komatsu, Solid State Ionics 179 (2008) 508–515.
[37] A. Yamada, S.C. Chung, K. Hinokuma, J. Electrochem. Soc. 148 (2001) A224–A229.
[38] H.-C. Kang, D.-K. Jun, B. Jin, E.M. Jin, K.-H. Park, H.-B. Gu, K.-W. Kim, J. Power Sources 179 (2008) 340–346.
[39] S.S. Zhang, J.L. Allen, K. Xu, T.R. Jow, J. Power Sources 147 (2005) 234–240.
[40] S.J. Kwon, C.W. Kim, W.T. Jeong, K.S. Lee, J. Power Sources 137 (2004) 93–99.